JACS
JOURNAL OF THE AMERICAN CHEMICAL SOCIETY

ARTICLE

pubs.acs.org/JACS

Initial Growth of Lutetium(III) Bis-phthalocyanine on Ag(111) Surface

Marius Toader,[†] Martin Knupfer,[§] Dietrich R. T. Zahn,[‡] and Michael Hietschold*[,†]

[†]Institute of Physics, Solid Surfaces Analysis Group, and [‡]Institute of Physics, Semiconductor Physics, Chemnitz University of Technology, D-09107 Chemnitz, Germany

[§]Leibniz Institute for Solid State and Materials Research, IFW Dresden, D-01171 Dresden, Germany

Supporting Information

ABSTRACT: The adsorption of lutetium(III) bis-phthalocyanine ($LuPc_2$) on Ag(111) was investigated using scanning tunneling microscopy and spectroscopy (STM/STS). A comprehensive study was carried out toward understanding the driving mechanism responsible for the formation of the first and second monolayers (MLs). In both MLs, the adsorbed molecules are found to exhibit different in-plane orientations arranged according to a "chess-board" like pattern. Highly resolved STM images allowed an exact determination of the corresponding angle mismatch, which differs for the first and second MLs. The tunneling transport through individual molecules reveals a negative differential resistance (NDR) effect detectable within the current−voltage curves. The corresponding density of states (DOS) representation is consistent with a resonant tunneling mechanism sustained by the valence band (VB) states close to the Fermi energy (E_F) recorded via highly resolved ultraviolet photoemission spectroscopy (UPS).

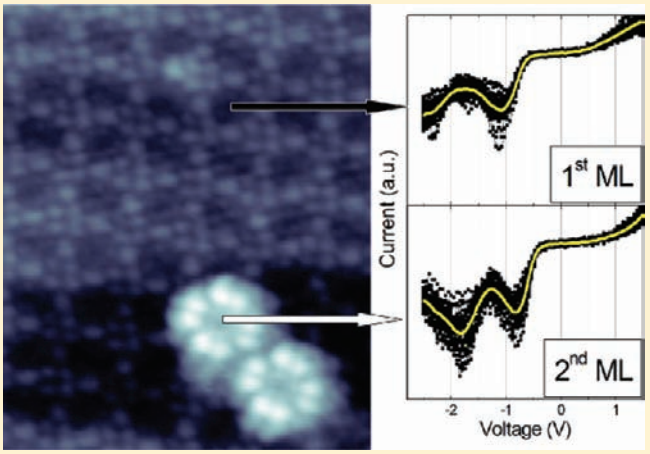

INTRODUCTION

Because of the strong demand of nanoscale technology for novel, low-dimensional active elements, single molecular magnets (SMM) grew considerably in importance. There is a tremendous interest in research that addresses possible suitable candidates for spintronics applications. A controllable spin manipulation at single molecule level was recently reported via a chemical switch.[1] In this respect, rare earth (lanthanide) elements are of great interest due to their large magnetic moment and anisotropy. There are already reports that dedicate strategies toward SMM based on lanthanide ions.[2] The π-conjugated organometallic complexes such as lanthanide bis-phthalocyanines have been proven to behave as magnets at single molecule level.[3] Later, it was shown by the group of Ishikawa et al.[4] that these systems exhibit quantum tunneling magnetization. Moreover, such work could be extended to dinuclear lanthanide complexes with phthalocyaninato ligands.[5] Triple-decker complexes have been investigated[6] and reported to exhibit an electric-driven molecular switching effect at liquid/solid interfaces.[7] However, more extended work is dedicated to the double-decker SMM based on mononuclear lanthanide ions.[8,9] Their suitability for organic-based field effect transistors was probed as well.[10,11] Corresponding properties like photosensitivity[12] and magnetic response[13] have been successfully enhanced in hybrid complexes using carbon nanotubes. However, outstanding performance of molecule-based nanodevices will strongly depend on the interfaces formed upon adsorption on distinct inorganic substrates, where the morphological and electronic properties deviate considerably with respect to bulk-like thick films. Therefore, a comprehensive understanding of organic/inorganic interface formation in the initial growth phase is needed. A preservation of the magnetic behavior was reported for adsorbed double-decker $TbPc_2$[14,15] on metal surfaces. This is of great advantage as compared to the single plane counterpart CoPc where the magnetic spin is quenched for the first monolayer (ML).[16] Different works address the adsorption of distinct lanthanide-based bis-phthalocyanine complexes using STM.[17−20] However, highly resolved extended molecular close-packed arrays (small domains are reported[19,20]) are still missing. Moreover, there is a question concerning the exact in-plane orientation within highly dense-packed structures. Information concerning the second ML formation in terms of morphology and electronic behavior is still missing as well. Therefore, in this work, the adsorption of lutetium(III) bis-phthalocyanine ($LuPc_2$) on Ag(111) substrate is investigated. Distinct aspects concerning the morphology and electronic properties are addressed for the first and second MLs, and the observed deviations are discussed.

Received: January 7, 2011
Published: March 18, 2011

dx.doi.org/10.1021/ja200168a | J. Am. Chem. Soc. 2011, 133, 5538–5544

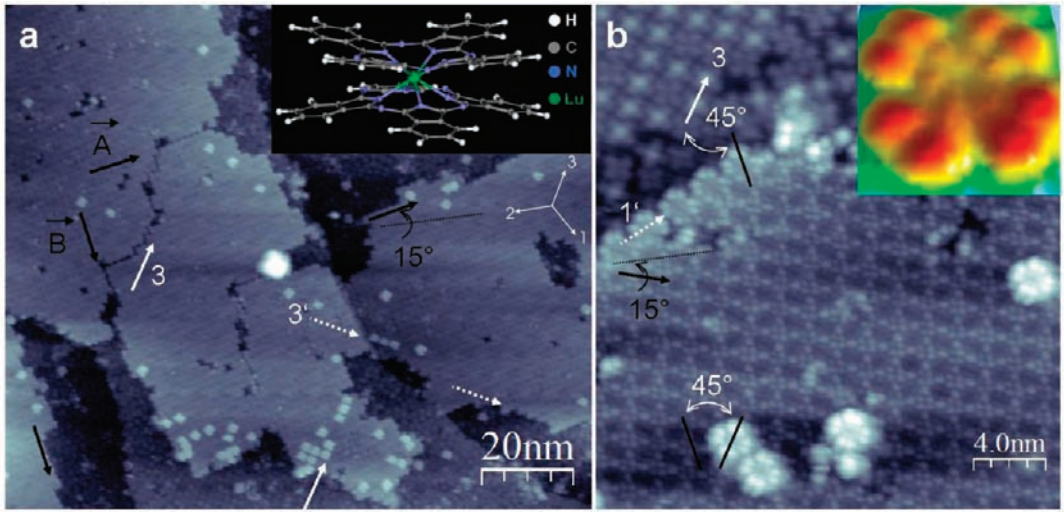

Figure 1. STM images for $LuPc_2$ adsorbed on Ag(111) recorded in constant current mode using a tunnelling current of 100 pA and a sample bias of −1 V (the inset shows the corresponding molecular structure for $LuPc_2$ (a)), and of −2 V (the inset shows a highly resolved isolated molecule where the submolecular features are consistent with the delocalized π systems (b)).

EXPERIMENTAL DETAILS

A variable-temperature STM (Omicron GmbH) operating under ultrahigh vacuum (UHV) conditions (base pressure $\leq 2 \times 10^{-10}$ mbar) was used for recording the data presented. All STM/STS results were achieved at a corresponding temperature of 30 K. Electrochemically etched tungsten tips (cut from a polycrystalline W wire) were used. The STS data were recorded using single point spectroscopy by positioning the tip on top of the molecular center. Each single ST spectrum shown is averaged over approximately 40 curves obtained from adjacent molecules. The photoemission spectroscopy (PES) data were recorded in the normal emission (NE) mode at room temperature (RT) under similar UHV conditions. A photon energy of 55 eV was used to obtain the valence band PES data. The PES experiments were carried out at the Material Science end-station at the Elettra synchrotron radiation facility in Trieste. For both types of experiments, the same Knudsen cell was used to evaporate the molecules via organic molecular beam deposition. A relatively high deposition rate ~0.5 nm/min (corresponding sublimation temperature of ~410 °C) was used to check the stability of the molecules during evaporation. Prior to deposition, the metal single crystal was cleaned in situ by repeated cycles of Ar^+ sputtering and subsequent annealing.

RESULTS AND DISCUSSION

The molecular structure for lutetium(III) bis-phthalocyanine is shown in the inset of Figure 1a. Two 4-fold π conjugated phthalocyanine ligands, rotated by 45° with respect to each other, are bridged via a Lu(III) ion. When adsorbed on the Ag(111) surface, extended molecular arrays are formed (see the large scale STM image in Figure 1a). The presence of uncovered areas between molecular domains indicates an attractive molecule−molecule interaction (see the black arrows that point along the unit cell vectors). In good agreement with previous reports, which address the adsorption of similar YPc_2 on Au(111),[19] the smallest angle mismatch between one unit cell vector and one of the equivalent substrate directions was determined to be 15° (see Figure 1a and b). Moreover, well-defined domain edges are found to develop as well along the close-packed directions of the substrate (e.g., $[1\bar{1}0]$) (see the white solid arrow) or along the corresponding perpendicular directions (e.g., $[11\bar{2}]$) (see the white dotted arrow). This suggests that a considerable contribution from the molecule−substrate interaction to the final packing mechanism exists. Consistent with the well-oriented sharp domain edges, molecular dot-chains are found to be formed within the second ML (marked by similar white arrows). Areas with a lower adsorption height (~1.4 Å) can be identified as well and are attributed to single-decker molecular domains formed via a thermal decomposition during evaporation. Therefore, the lutetium(III) bis-phthalocyanine is decomposed sometimes into two single-decker molecular species. One preserves the metal consistency leading to the formation of Lu(II) monophthalocyanine (LuPc), while the other ligand is metal-free and can be identified as a deprotonated phthalocyanine (*Pc* without the inner H atoms). The two species are easily distinguishable within highly resolved STM images due to their distinct molecular appearance of the central cavity at a negative bias voltage: bright protrusion for LuPc and shallow depression for *Pc* (see Figure 1b, top-left corner).

The appearance of lutetium monophthalocyanine is found to exhibit a strong bias polarity dependence, which is not the case for deprotonated *Pc* (see Supporting Information 1). The observation is presumably assigned to a higher density of filled states localized at the metal ion site, explained on the basis of a reduction effect of the Lu oxidation state via an electron flow from the substrate into the molecule mediated by the Lu ion and/or isoindole N. Similar voltage polarity dependence was previously reported for fluorinated cobalt phthalocyanine adsorbed on Ag(110).[21] Moreover, photoelectron spectroscopy has shown that there is also charge transfer to the metal center in the case of Co-porphyrins deposited on Ag(111), which supports our conclusion.[22] Ordered square structures are found via intermixing the two single-decker molecular species, which adsorb preferentially along the equivalent underlying directions and preserve the 4-fold symmetry within the formed arrays. The lutetium(III) bis-phthalocyanine molecular domains are easily distinguishable due to their relatively high adsorption height of ~4 ± 0.5 Å and distinct molecular appearance. Because of an effective decoupling from the surface states via the first *Pc* ring,

dx.doi.org/10.1021/ja200168a |*J. Am. Chem. Soc.* 2011, 133, 5538–5544

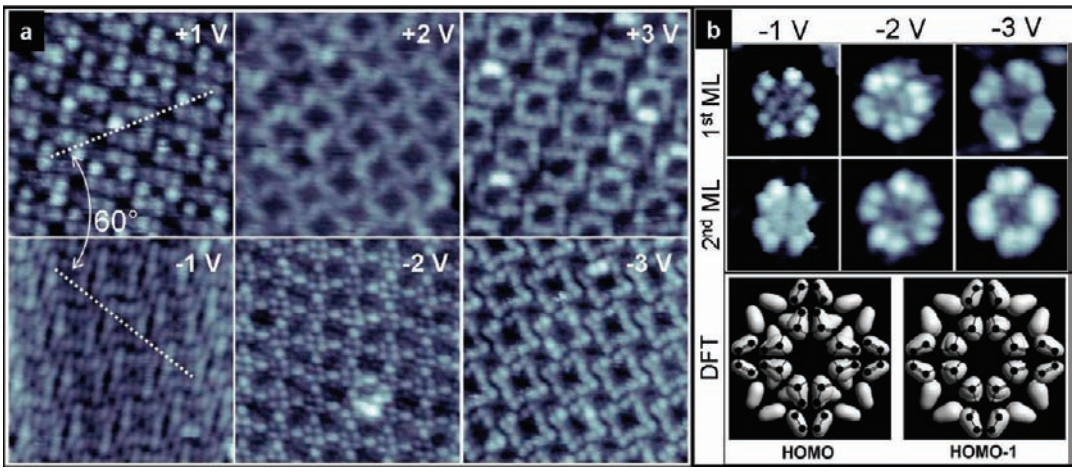

Figure 2. Voltage polarity dependence for molecular close-packed arrays within the first ML; each frame area is 10×10 nm^2 (a). Charge distribution within the molecular ligand for the filled states close to E_F determined experimentally for single molecules in the first ML (top) and second ML (middle) (each frame area is 3×3 nm^2) and theoretically for gas-phase isolated molecules (bottom) (b). For all frames, the tunnelling current was 100 pA.

the unperturbed π electronic clouds delocalized over the upper ligand determine the final molecular appearance. Highly resolved submolecular features for isolated molecules (see the inset of Figure 1b) are consistent with the 16 π electronic systems per upper ligand calculated using density functional theory (DFT) (see Figure 2b). However, due to the nonplanar geometry, the outer π electronic clouds appear brighter than the inner ones. Therefore, the molecules are mostly identified as eight-lobe structures (different from the four-lobe shape characteristic for the single-decker phthalocyanine). Still, a clear identification of individual molecules within densely packed arrays is very difficult at this bias voltage. Assigning the shallow depressions to individual central cavities, the counted features per molecule do not fit those identified for isolated molecules (minimum 8), because four surrounding features have coordination 1 while the other four have coordination 2 (see Figure 1b). Therefore, different in-plane orientations might be responsible for the lack of a precise identification, a fact that was only assumed in previous works.[19] As it will be shown later on, the validity of this assumption will be proven via a precise determination. Moreover, this effect is accompanied by an extended overlap of the molecular wave functions between neighboring molecules, creating a mixed and complicated contrast appearance of the submolecular features. The situation is different at the well-oriented domain edges where the in-plane orientation can be easily determined. The upper phthalocyanine ring was found to be rotated by 45° with respect to a close-packed orientation of the substrate. Because of the relative rotation of the two ligands (45°), the lower phthalocyanine ring is thus found to align one molecular axis with the underlying substrate direction. A considerable molecule−substrate interaction is found to contribute to the first ML formation via an overlapping between the π electronic clouds and surface states. Adsorbed via a $\pi-\pi$ stacking mechanism, the isolated molecules in the second ML are found to be rotated by 45° with respect to the underlying ones.

The contrast appearance of the molecular arrays within the first ML is found to be strongly dependent on the bias polarity (see Figure 2a, where all of the frames are equivalent and rotated by integers of 15° with respect to each other). Symmetric with respect to E_F, via increasing the absolute voltage value, the submolecular resolution is progressively lost.

Moreover, a better resolution is achieved at negative biases, most probably due to a higher symmetry close to the Fermi energy of the charge distribution within the molecular ligand for the filled orbitals (highest occupied molecular orbital HOMO/−1) as compared to the degenerated unfilled orbitals (lowest unoccupied molecular orbital LUMO/+1). Therefore, a detailed negative polarity dependence of the molecular appearance for isolated molecules within first and second MLs is shown in Figure 2b. The same contrast and light intensity were used to display the images (no artificial enhancement/reduction of the molecular appearance was introduced this way), which allow for a direct comparison. A similar charge distribution within the molecular ligand is reported independent of the investigated ML. Presumably, there is no (or very weak) influence of the substrate on the upper *Pc* ring. Via increasing the voltage, the outer π electronic clouds get broader, thus inducing a gradual quenching of the inner π orbitals. Consequently, a larger molecular appearance, which suppresses the submolecular features, considerably complicates an exact estimation of the in-plane orientation. The observations are consistent with the charge distribution contours for HOMO and HOMO−1 (calculated using Gaussian 03 software with the UB3LYP method and SDD basic sets) (see Figure 2b). Located at lower energies, the HOMO−1 orbital shows a more pronounced localization of the inner π electronic clouds to the C atoms directly bonded to the isoindole N and a corresponding broader appearance of the outer π orbitals. As the scenario indicates, a study at lower bias voltages enables a higher submolecular resolution. However, despite our previous observation that there is no (or very weak) influence of the substrate on the upper *Pc* ring, an increasingly pronounced asymmetry of the molecule orbitals within the first ML is found, which is less noticeable within the second ML. The effect is due to the organic radical delocalized over the two *Pc* rings characteristic for the neutral lanthanide-based bis-phthalocyanines,[23] which favors an intramolecular interaction between the ligands. Similar to the nonplanar MePc,[24] the first *Pc* ligand direct in contact with the metal surface is reasonably expected to exhibit a slight geometry distortion upon adsorption. Moreover, different atomic configuration underneath the molecular backbone (as a consequence of the previously discussed alignment with the underlying substrate

dx.doi.org/10.1021/ja200168a |*J. Am. Chem. Soc.* 2011, 133, 5538–5544

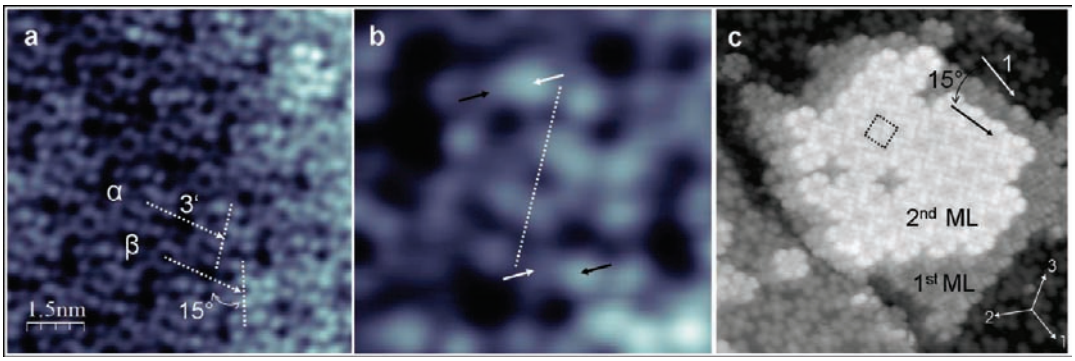

Figure 3. Highly resolved STM images for molecular close-packed array in the first ML, −0.5 V, 100 pA (a); for α molecule, 3 × 3 nm^2 (b); and for molecular close-packed array in the second ML, −1 V, 100 pA, 20 × 20 nm^2 (c).

directions) will enable a different molecule−substrate coupling along the two molecular axes. Consequently, an adsorption-induced asymmetry of the first *Pc* ring is propagated to the top *Pc* ligand as a result of the intramolecular interaction. However, the interface confined effect is less noticeable within the second ML, which is effectively decoupled from the substrate via the first ML that acts as a buffer layer. The effect may have strong consequences on the self-assembly process and the corresponding electrical response of the molecules adsorbed within different layers, as will be shown later.

A high magnification of a molecular close-packed array within the first ML is shown in Figure 3a, where a negative bias voltage of −0.5 V was used for recording. As predicted by the polarity dependence study, at this relatively low voltage, the molecular features are imaged with optimum sharpness and localization. The inner π orbitals are considerably enhanced, while the outer ones get better defined. Even though unresolved individually, the inner π systems appear as an inner ring. Efficiently, the different in-plane orientations are determined with high accuracy. Differently oriented molecules (α and β) with an in-plane angle mismatch of 15° are found to arrange according to a "chess-board" like pattern. The estimated angle is consistent with the previously determined minimum mismatch between the unit cell vector and one equivalent substrate direction. Moreover, this angle is different from the one proposed in ref 19, where an angle of 30° was used for modeling the molecular structure. However, we do not question the proposed model because the lower reactivity of the Au(111) surface might have a lower impact on the final structure. The subsequent types of molecular rows (α and β) are reported to be well oriented (see Figure 3a), which justifies the presence of previously discussed sharp domain edges, which always appear along the diagonal of the molecular unit cell. For an overview of the lattice parameters and proposed model, see Supporting Information 2. Interestingly, the submolecular features do not exhibit a similar equivalent contrast appearance. A high magnification of one α type molecule is shown in Figure 3b. A noticeable nonequivalent contrast is reported for the diagonally opposite features marked by white arrows. Correspondingly, the neighbor β type molecules manifest an opposite effect (refer to the black arrows). Presumably, the molecular features at the periphery have the same charge consistency (π character). Therefore, excluding an electronic effect, the observed nonequivalent contrast might be exclusively attributed to a slight geometrical distortion of the upper *Pc* ligand, most probably due to a steric repulsion as well as due to the previously discussed intramolecular interaction. Additional contribution might occur from a vertical $\pi-\pi$ interaction between upper and lower *Pc* ligands of neighboring molecules. Such an extended three-dimensional (3D) molecule−molecule interaction is highlighted for the double-decker molecules, which presents a real novelty as compared to single-decker counterparts, which manifest an exclusively in-plane interaction. Therefore, an extended overlap of the molecular wave functions enhances particular submolecular features to the detriment of other ones. Consequently, the difficulties encountered for these systems are justified for a precise assignment of the in-plane orientation within closely packed arrays. As previously mentioned, the isolated molecules in the second ML adsorb exactly on top of the underlying ones. Therefore, densely packed molecular arrays within second ML are formed according to a similar growth mechanism (see Figure 3c). An equivalent molecular lattice is achieved where molecules with different in-plane orientation arrange according to a similar "chess-board" like pattern. However, the angle mismatch in the second ML is reduced to one-half (7.5°) as compared to the first ML. For a higher resolution of the second ML and a corresponding assignment of the in-plane orientation, refer to Supporting Information 3. The isolated molecules in the second ML (reported previously to exhibit a relative 45° rotation) rearrange the in-plane orientation within densely packed arrays, reaching a compromise driven by an additional molecule−molecule interaction. The small deviations observed for the second ML are assigned to a perturbed fine balance between the molecule−substrate and molecule−molecule interaction. The first type of driving force is considerably reduced, while the second one grows in importance.

The tunnelling transport through individual molecules adsorbed within first and second MLs is found to manifest negative slopes within the corresponding current−voltage curves (Figure 4a). Known as the negative differential resistance (NDR) effect, the reported phenomenon is of great interest for electronic applications. Present in doped silicon,[25,26] the NDR was reported theoretically[27] and experimentally[28,29] to be induced in organic-based hybrid devices as well. Moreover, multiple NDR events at single molecule level were reported to appear selectively as a function of the silicon doping type.[30] Hence, the effect was observed only for negative sample bias on n-type silicon and for positive sample bias on p-type silicon. For single-decker cobalt phthalocyanine adsorbed on Au(111), the NDR occurs only in the part of negative sample bias and only for nickel tips positioned on top of the cobalt ion.[31] Absent for tungsten

dx.doi.org/10.1021/ja200168a |*J. Am. Chem. Soc.* 2011, 133, 5538–5544

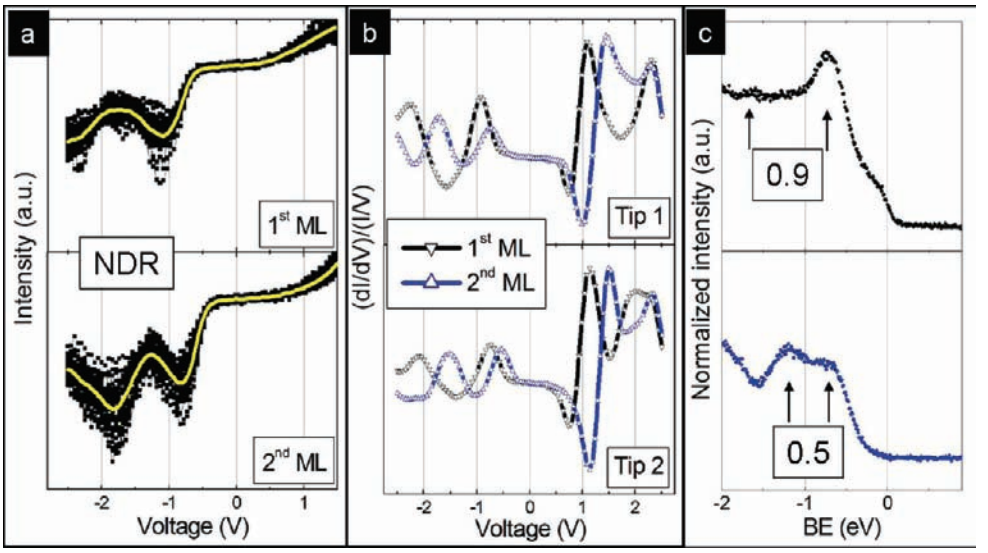

Figure 4. Current−voltage curves recorded at single molecule level reveal NDR behavior, −1 V, 100 pA (a); the corresponding DOS representation (b); and VB spectra in the Fermi energy region recorded using synchrotron radiation (55 eV) for 0.7 nm (top) and 1.3 nm (bottom) of $LuPc_2$ adsorbed on Ag(111) (BE = binding energy) (c).

tips, the effect was explained on the basis of a mechanism originating from a local orbital symmetry matching. To our knowledge, the NDR response in tunnelling transport through individual lanthanide-based bis-phthalocyanines has not been previously reported. One and two negative slopes were found to appear in the negative part of the sample bias for the first and second MLs, respectively (see Figure 4a). However, independent of the ML, two minima are identified within the investigated negative voltage range (−2.5 ÷ 0 V). The corresponding energy separation is reduced via increasing the thickness. The behavior is consistent and strongly correlated with the observed deviation of the energy level positions encountered for the first and second MLs (Figure 4b). At a negative sample bias, the contribution to the tunnelling current comes mainly from the occupied states of the molecule. The first two occupied levels below E_F are assigned to HOMO and HOMO−1 orbitals. As it was shown in the previous discussion, there is an effective coupling between the first *Pc* ligand and metal surface states, which drives (contributes to) the self-assembly mechanism. It is reasonable to assume a molecule−substrate interaction mainly driven by the N atoms, which are the main electron acceptors of the molecules. Therefore, a charge redistribution at the corresponding atom site is likely to appear. Consequently and consistent with this assumption, the HOMO−1 (found to be more localized at the C site directly bonded to the isoindole N) is located at lower energy for the first ML as compared to the second ML. As previously mentioned, the intramolecular interaction is effectively propagating the substrate influence on the final electrical response of the molecules adsorbed within the first ML. Still, the effect is considerably reduced for the second ML, which is decoupled from the substrate via the first ML. However, this considerable difference is relatively small for HOMO level, because the inner π orbitals are more delocalized. The tip apex was slightly changed via an in situ local melting procedure to determine the corresponding influence on the energy level alignment. The results are found to be very similar independent of the tip shape (see Figure 4b). The occupied states, directly involved in the tunnelling transport, are reported to be more affected (an unidirectional

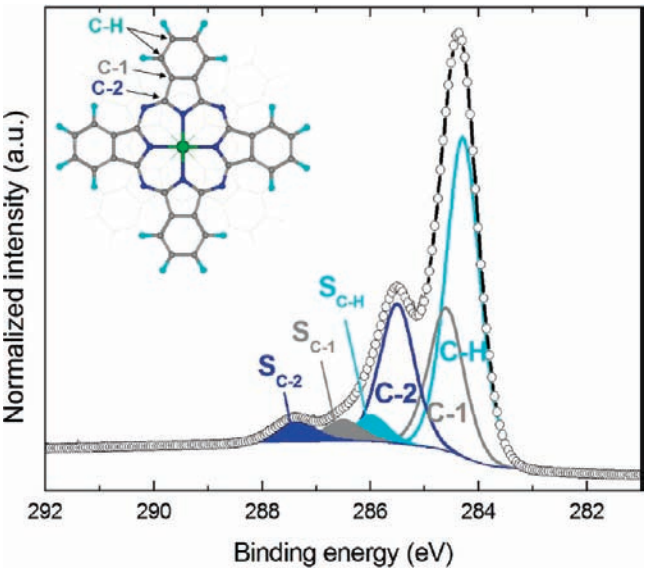

Figure 5. C 1s core level spectra for 1.3 nm of $LuPc_2$ adsorbed on Ag(111) measured using synchrotron radiation (450 eV); the inset depicts the molecular structure for $LuPc_2$ where the top *Pc* ligand is enhanced and the corresponding different types of C atoms are indicated.

shift toward higher energies with corresponding values in the range of 0.18 ÷ 0.21 eV) as compared to the almost undisturbed unoccupied states (similar shift in the range of 0.04 ÷ 0.05 eV). Therefore, in the following sequence, the discussed values obtained with tip #2 will be given in brackets. As already mentioned, the HOMO − HOMO−1 energy separation is reduced from 1.38 (1.36) eV for the first ML to 0.99 (0.99) eV for the second ML. Independent of the tip shape and corresponding introduced small shifts, the previously discussed energy separation is reproduced with a high accuracy. To check the observed behavior, highly resolved valence band spectra in the

dx.doi.org/10.1021/ja200168a |*J. Am. Chem. Soc.* 2011, 133, 5538–5544

Fermi level region were recorded for two molecular thicknesses using synchrotron radiation (see Figure 4c). A similar reduction of the HOMO − HOMO−1 energy separation is demonstrated via increasing the film thickness. The smaller values are mainly attributed to the averaging character of the photoemission technique. Therefore, an averaged signal extended over decomposed molecules and molecular domains formed at surface defect sites might introduce the reported deviations. However, the UPS data are of great importance to sustain a resonant tunnelling mechanism responsible for the observed NDR effect. This type of mechanism was used previously[30] to explain the origin of the NDR. Moreover, the current−voltage behavior as a function of molecular film thickness is highly consistent with the evolution of the energy level alignment at the organic/metal interface determined using STS and UPS. Additionally, the energy separation between the first unfilled levels above Fermi was determined to be 1.17 eV (1.14 eV assuming a shift similar to the one reported for tip #1) for the first ML and 0.75 (0.75) eV for the second ML. The averaged molecular gap is estimated to be 1.97 and 2.16 eV for the first and second MLs, respectively. Because of the unsignificantly small shifts introduced by the tip shape for the empty states, the molecular gap was estimated with an averaged error bar not exceeding 0.1 eV. Additionally, these values are consistent with the energy splitting (1.7 ÷ 1.9 eV) between the main core level components and corresponding shakeup satellites determined from the C 1s spectra (see Figure 5).

Besides the main core level components, shakeup satellites are identified at higher energies caused by a kinetic-energy loss of photoelectrons via simultaneously excited $\pi-\pi^*$ transitions.[32] Assigned as transitions from the highest occupied molecular orbital (HOMO) to the lowest unoccupied molecular orbital (LUMO), the energy splitting between the main core level components and the corresponding satellite features can be considered as an estimative value for the molecular gap.[33] A value of 2:1.98:4.20 is reported for the fitted intensity ratio described as $(C\text{-}1+S_{C\text{-}1}):(C\text{-}2+S_{C\text{-}2}):(C-H+S_{C-H})$, which is in very good agreement with the numerical ratio of distinct types of carbon atoms identified within the molecular ligand, 2:2:4 (C1:C2:C−H), denoting that a further decomposition of monophthalocyanine species is not likely to appear.

CONCLUSIONS

The initial growth of lutetium(III) bis-phthalocanine on Ag(111) is found to be of high complexity in terms of morphology and electronic properties. A fine balance between the molecule−substrate and molecule−molecule interaction drives the molecular self-assembly. Molecules adopting different in-plane orientation are reported to arrange according to a "chess-board" like pattern where an extended 3D molecule−molecule interaction was found. An exact determination of the angle mismatch was reported for the first (15°) and second (7.5°) MLs. There is no (or very weak) substrate influence on the upper ligand, which manifests a similar charge distribution independent of the adsorbed ML. However, a considerable coupling was found between the molecular orbitals of the first *Pc* ligand and the metal surface states. Consequently, the energy level positions are different for the molecules adsorbed within the first or second MLs. The tunnelling transport at the single molecule level is reported to show a NDR behavior enlarging the great application potential of lanthanide-based bis-phthalocyanine toward logic/memory devices. The observed phenomenon is consistent with a resonant tunnelling mechanism sustained by the STS and UPS data.

ASSOCIATED CONTENT

Supporting Information. Voltage polarity dependence of the appearance of single-decker phthalocyanine species. Lattice parameters and proposed structural model. High magnification of one molecular domain edge within the second ML. This material is available free of charge via the Internet at http://pubs.acs.org.

AUTHOR INFORMATION

Corresponding Author
hietschold@physik.tu-chemnitz.de

ACKNOWLEDGMENT

This work was supported by the Deutsche Forschungsgemeinschaft (DFG) through GRK 1215 "Materials and Concepts for Advanced Interconnects" and Research Unit 1154 "Towards Molecular Spintronics". We thank P. Shukrynau for technical support. Concerning the photoemission data, we also thank T. Toader for fruitful discussions and M. Vondráček for technical support.

REFERENCES

(1) Wäckerlin, C.; Chylarecka, D.; Kleibert, A.; Müller, K.; Iacovita, C.; Nolting, F.; Jung, T. A.; Ballav, N. *Nat. Commun.* **2010**, *1*, 61.
(2) Sessoli, R.; Powell, A. K. *Coord. Chem. Rev.* **2009**, *253*, 2328.
(3) Ishikawa, N.; Sugita, M.; Ishikawa, T.; Koshihara, S.; Kaizu, Y. *J. Am. Chem. Soc.* **2003**, *125*, 8694.
(4) Ishikawa, N.; Sugita, M.; Wernsdorfer, W. *Angew. Chem.* **2005**, *117*, 2991.
(5) Ishikawa, N. *Polyhedron* **2007**, *26*, 2147.
(6) Yoshimoto, S.; Sawaguchi, T.; Su, W.; Jiang, J.; Kobayashi, N. *Angew. Chem., Int. Ed.* **2007**, *46*, 1071.
(7) Lei, S.-B.; Deng, K.; Yang, Y.-L.; Zeng, Q.-D.; Wang, C.; Jiang, J.-Z. *Nano Lett.* **2008**, *8*, 1836.
(8) Gonidec, M.; Luis, F.; Vílchez, .; Esquena, J.; Amabilino, D. B.; Veciana, J. *Angew. Chem., Int. Ed.* **2010**, *49*, 1623.
(9) AlDamen, M. A.; Clemente-Juan, J. M.; Coronado, E.; Martí-Gastaldo, C.; Gaita-Arinño, A. *J. Am. Chem. Soc.* **2008**, *130*, 8874.
(10) Su, W.; Jiang, J.; Xiao, K.; Chen, Y.; Zhao, Q.; Yu, G.; Liu, Y. *Langmuir* **2005**, *21*, 6527.
(11) Katoh, K.; Yoshida, Y.; Yamashita, M.; Miyasaka, H.; Breedlove, B. K.; Kajiwara, T.; Takaishi, S.; Ishikawa, N.; Isshiki, H.; Zhang, Y. F.; Komeda, T.; Yamagishi, M.; Takeya, J. *J. Am. Chem. Soc.* **2009**, *131*, 9967.
(12) Cao, L.; Chen, H.-Z.; Zhou, H.-B.; Zhu, L.; Sun, J.-Z.; Zhang, X.-B.; Xu, J.-M.; Wang, M. *Adv. Mater.* **2003**, *15*, 909.
(13) Kyatskaya, S.; Mascarós, J. R. G.; Bogani, L.; Hennrich, F.; Kappes, M.; Wernsdorfer, W.; Ruben, M. *J. Am. Chem. Soc.* **2009**, *131*, 15143.
(14) Vitali, L.; Fabris, S.; Conte, A. M.; Brink, S.; Ruben, M.; Baroni, S.; Kern, K. *Nano Lett.* **2008**, *8*, 3364.
(15) Stepanow, S.; Honolka, J.; Gambardella, P.; Vitali, L.; Abdurakhmanova, N.; Tseng, T.-C.; Rauschenbach, S.; Tait, S. L.; Sessi, V.; Klyatskaya, S.; Ruben, M.; Kern, K. *J. Am. Chem. Soc.* **2010**, *132*, 11900.
(16) Chen, X.; Fu, Y.-S.; Ji, S.-H.; Zhang, T.; Cheng, P.; Ma, X.-C.; Zou, X.-L.; Duan, W.-H.; Jia, J.-F.; Xue, Q.-K. *Phys. Rev. Lett.* **2008**, *101*, 197208.
(17) Ye, T.; Takami, T.; Wang, R.; Jiang, J.; Weiss, P. S. *J. Am. Chem. Soc.* **2006**, *128*, 10984.

(18) Miyake, K.; Fukuta, M.; Asakawa, M.; Hori, Y.; Ikeda, T.; Shimizu, T. *J. Am. Chem. Soc.* **2009**, *131*, 17808.
(19) Zhang, Y. F.; Isshiki, H.; Katoh, K.; Yoshida, Y.; Yamashita, M.; Miyasaka, H.; Breedlove, B. K.; Kajiwara, T.; Takaishi, S.; Komeda, T. *J. Phys. Chem. C* **2009**, *113*, 9826.
(20) Zhang, Y.; Guan, P.; Isshiki, H.; Chen, M.; Yamashita, M.; Komeda, T. *Nano Res.* **2010**, *3*, 604.
(21) Toader, M.; Gopakumar, T. G.; Abdel-Hafiez, M.; Hietschold, M. *J. Phys. Chem. C* **2010**, *114*, 3537.
(22) Bai, Y.; Buchner, F.; Kellner, I.; Schmid, M.; Vollnhals, F.; Steinrück, H.-P.; Marbach, H.; Gottfried, J. M. *New J. Phys.* **2009**, *11*, 125004.
(23) Ishikawa, N.; Sugita, M.; Tanaka, N.; Ishikawa, T.; Koshihara, S.; Kaizu, Y. *Inorg. Chem.* **2004**, *43*, 5498.
(24) Toader, M.; Hietschold, M. *J. Phys. Chem. C* **2011**, *115*, 3099.
(25) Bedrossian, P.; Chen, D. M.; Mortensen, K.; Golovchenko, J. A. *Nature* **1989**, *342*, 258.
(26) Lyo, I.-W.; Avouris, P. *Science* **1989**, *245*, 1369.
(27) Ribeiro, F. J.; Lu, W.; Bernholc, J. *ACS Nano* **2008**, *2*, 1517.
(28) Chen, J.; Reed, M. A.; Rawlett, A. M.; Tour, J. M. *Science* **1999**, *286*, 1550.
(29) Yoon, W.-J.; Chung, S.-Y.; Berger, P. R.; Asar, S. M. *Appl. Phys. Lett.* **2005**, *87*, 203506.
(30) Guisinger, N. P.; Greene, M. E.; Basu, R.; Baluch, A. S.; Hersam, M. C. *Nano Lett.* **2004**, *4*, 55.
(31) Chen, L.; Hu, Z.; Zhao, A.; Wang, B.; Luo, Y.; Yang, J.; Hou, J. G. *Phys. Rev. Lett.* **2007**, *99*, 146803.
(32) Peisert, H.; Knupfer, M.; Schwieger, T.; Fuentes, G. G.; Olligs, D.; Fink, J.; Schmidt, Th. *J. Appl. Phys.* **2003**, *93*, 9683.
(33) Piper, L. F. J.; Cho, S. W.; Zhang, Y.; DeMasi, A.; Smith, K. E.; Matsuura, A. Y.; McGuinness, C. *Phys. Rev. B* **2010**, *81*, 045201.